Chapter 20

Probing Amyloid-DNA Interaction with Nanofluidics

Rajib Basak, Indresh Yadav, Véronique Arluison, Jeroen A. van Kan, and Johan R. C. van der Maarel

Abstract

Nanofluidics is an emerging methodology to investigate single biomacromolecules without functionalization and/or attachment of the molecules to a substrate. In conjunction with fluorescence microscopy, it can be used to investigate structural and dynamical aspects of amyloid-DNA interaction. Here, we summarize the methodology for fabricating lab-on-chip devices in relatively cheap polymer resins and featuring quasi one-dimensional nanochannels with a cross-sectional diameter of tens to a few hundred nanometers. Site-specific staining of amyloid-forming protein Hfq with a fluorescence dye is also described. The methodology is illustrated with two application studies. The first study involves assembling bacterial amyloid proteins such as Hfq on double-stranded DNA and monitoring the folding and compaction of DNA in a condensed state. The second study is about the concerted motion of Hfq on DNA and how this is related to DNA's internal motion. Explicit details of procedures and workflows are given throughout.

Key words nucleoid-associated protein, DNA, fluorescence, Brownian motion

1 Introduction

Over the past two decades, advances in nanolithography have made it possible to fabricate devices that have at least one dimension at the nanoscale. In combination with fluids, these so-called nanofluidic devices have found widespread applications in the fields of, among others, chemistry, molecular biology, material science, and medicine [1]. Since the nanoscale dimension is on the order of or smaller than the typical size of biomacromolecules (e.g., proteins and DNA), they provide an excellent tool for the investigation and manipulation at the single-molecule level [2, 3]. Specific advantages of nanofluidics are that the molecules can be investigated without functionalization, such as attachment of colloidal beads and that they are usually entropically trapped without the grafting or attachment to a substrate. The methodology described in the present chapter is based on stretching single DNA molecules on a parallel array of long and rectangular nanofluidic channels. The

Véronique Arluison et al. (eds.), *Bacterial Amyloids: Methods and Protocols*,
Methods in Molecular Biology, vol. 2538, https://doi.org/10.1007/978-1-0716-2529-3_20,

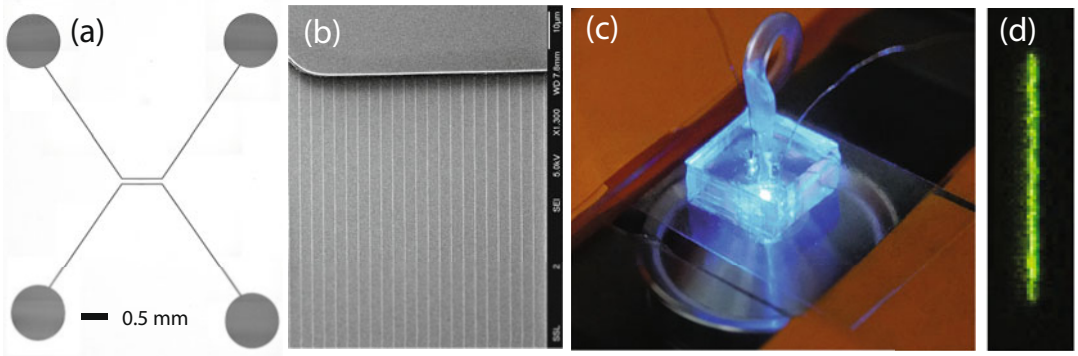

Fig. 1 (**a**) Optical image of the V-shape feeding microchannel mold. (**b**) Scanning electron microscopy image of the nanochannel array in hydrogen silsesquioxane (HSQ). (**c**) Image of lab-on-chip device mounted on an inverted microscope slide. (**d**) Fluorescence image of bacteriophage T4-DNA stained with YOYO-1 dye and confined to a channel with a cross-section of 250 × 250 nm^2

channels are quasi one-dimensional, have a cross-sectional diameter of tens to a few hundreds of nanometers, and are integrated in lab-on-chip devices. Relatively high throughput can be achieved by using an array consisting of a few tens of channels. The DNA molecules and proteins are stained with fluorescence dyes and imaged using fluorescence microscopy. An illustration of the experimental setup is shown in Fig. 1.

Nanofluidic devices have extensively been used to investigate the conformational response of DNA to changes in the surrounding buffer medium such as ionic strength, presence of binding and nonbinding ligands, and crowding agents [3, 4]. They have also been used for large-scale mapping of genomic information, either of DNA in double- or single-stranded form [5–7]. Here, we will first describe the experimental method, including materials and setup. The methodology will further be illustrated with two relatively recent application studies in the context of bacterial protein-DNA interaction. More precisely, we will follow the assembly of bacterial amyloid proteins such as Hfq on DNA and monitor the folding and compaction of DNA in a condensed state [8–11]. We will also measure the diffusion of Hfq on DNA and how this relates to DNA's internal motion [12, 13].

2 Materials

2.1 DNAs and Proteins

1. Bacteriophage λ-DNA (48.5 kbp).
2. Bacteriophage T4-DNA (166 kbp.
3. T-buffer: 10 mM Tris–HCl pH 8.0, and 1 mM EDTA.
4. YOYO-1 dye.
5. Bacterial amyloid of interest.

6. T4-DNA ligase.
7. Micro-dialyzer.
8. Tris[2-carboxyethyl] phosphine (TCEP), 10 mM.
9. Cy3 or Cy5-maleimide (*see* **Note 1**).
10. Ni-NTA resin.
11. Dimethyl sulfoxide DMSO.
12. Washing buffer: 20 mM Tris–HCl pH 8.0, 20 mM imidazole, 0.3 M NaCl.
13. Elution buffer: 20 mM Tris–HCl pH 8.0, 500 mM imidazole, 0.3 M NaCl.

2.2 Nanofluidic Devices

The two-step fabrication process is described in Subheading 3.1 *(see* **Note 2***)*

1. Hydrogen silsesquioxane (HSQ) resist (Dow Corning, Midland, MI).
2. mr-DWL photoresist (Micro Resist Technology, Berlin, Germany).
3. Prepolymer of polydimethylsiloxane (PDMS) and curing agent (Sylgard, Dow Corning).
4. PDMS with enhanced elasticity modulus (X-PDMS, SCIL Nanoimprint solutions, Eindhoven, the Netherlands).
5. Poly(methyl methacrylate) (PMMA).
6. Inorganic-organic hybrid polymer OrmoStamp (Micro Resist Technology).
7. Anti-stiction coating (teflon or diamond-like carbon).
8. Nanolithography facility with access to laser and either proton or electron beam writing.
9. Atomic force (AFM) and scanning electron microscopy (SEM).
10. Nano-imprinter.
11. Spin-coater.
12. Plasma cleaner.
13. Glass coverslips.

2.3 Experimental Setup

1. Inverted fluorescence microscope such as Nikon Eclipse Ti with a 100 times oil immersion objective (numerical aperture 1.49).
2. Illumination by 200-mW/488-nm (YOYO- 1), 400 mW/556-nm (Cy3), and 200 mW/640-nm lasers, and a 405/488/561/640-nm filter cube.
3. A source meter (power supply) with a voltage in the range 0.1–100 V.
4. Platinum electrodes.

5. An electron multiplying charge-coupled device (EMCCD) camera such as iXon X3 (Andor Technology, Belfast, UK).
6. Software for image acquisition such as NIS-Element.
7. Software for image analysis such as MATLAB (MathWorks, Natick, MA).

3 Methods

3.1 Preparation of the Nanofluidic Devices

First, a master mold pattern is produced using nanolithography. Second, this master is replicated on a polymer, which allows the preparation of multiple replicas and, accordingly, offers the opportunity to use a fresh chip for each experiment.

3.1.1 Fabrication of the Master Mold Pattern

Our nanofluidic devices feature both nano- and microfluidic patterns. Both patterns should be imprinted and superposed on a substrate like silicon. The structural layout of the master stamp is shown in Fig. 1.

1. The nanofluidic pattern is prepared on spin-coated HSQ resist with either proton or electron beam writing [14, 15]. The height and width of the nanochannel features are typically tens to a few hundreds of nm. The length of the channels is generally 50–100 μm.
2. The dimensions of the nanofluidic pattern can be quantified with AFM and SEM.
3. The nanofluidic patterns are connected to the loading reservoirs through a superposing microfluidic pattern. The microfluidic pattern can be fabricated and aligned with a laser writer on mr-DWL photoresist.
4. The master stamp is coated with an anti-stiction layer of a few nanometer. A 5 nm Teflon or diamond-like carbon layer will facilitate the release of the replicated polymer chips.

3.1.2 Chip Replication

The replication process depends on the properties of the polymer. We use PDMS, PDMS with enhanced elasticity modulus (X-PDMS), and PMMA.

1. To prepare a chip in PDMS, the master stamp is replicated in PDMS followed by curing with curing agent at 65 °C (338 K) for a minimum of 12 h. These replicas are sealed with a glass coverslip following plasma oxidation of both substrates. The coverslip can also be coated with a layer of PDMS, resulting in rectangular channels fully lined with PDMS. PDMS is suitable for larger channel diameters exceeding, say 200 nm. For smaller channel cross-sections, PDMS tends to collapse due to its relatively soft elasticity.

2. The collapse for smaller channel diameters can be avoided by using PMMA, which has a higher elasticity modulus compared to PDMS. For PMMA chip fabrication, the carbon-coated master stamp is first copied in an inorganic-organic hybrid polymer OrmoStamp using a UV-based nanoimprinting lithography. The copied stamp is used to thermally imprint on a 175 μm thick PMMA film with a nano-imprinter. The imprinted film is then sealed with a 500 μm thick PMMA film by applying elevated pressure. A drawback of PMMA is (significant) auto-fluorescence, which becomes problematic in the face of weak fluorescence dyes.
3. Channel collapse can also be avoided by using X-PDMS. A thin layer of X-PDMS is spin-coated on the OrmoStamp mold and cured at 50 °C for 3 min. The channel features are hence imprinted in X-PDMS. The X-PDMS spin-coated and cured OrmoStamp mold is covered with a layer of regular PDMS and cured with a curing agent at 65 °C for a minimum of 12 h. The replicas are sealed with (X-PDMS coated) glass coverslips following plasma oxidation of replica and coverslip. X-PDMS chips are the workhorse for channels with a diameter in the range 50–150 nm.

3.2 Preparation of Covalently Bonded Concatemers of λ-DNA

Covalently bonded concatemers of λ-DNA can be prepared by ligating the cohesive ends of the λ-DNA with T4-DNA ligase. The ligation process is carried out overnight at 4 °C with 10 U of T4 DNA ligase to ligate 1 microgram of lambda DNA. DNA ligase was then inactivated by heating the sample at 65 °C for 10 min. Finally, the sample needs to be dialyzed in a micro-dialyzer and re-dispersed in T-buffer.

3.3 Preparation of Fluorescence-Labeled Protein

3.3.1 Choice of Labeling Position

Site-specific conjugation on a cysteine can be achieved with a maleimide-ester dye that forms a covalent bond with the cysteine sulfhydryl group. Maleimide-linked cyanine dyes are readily available from different companies. Note that cysteine can be absent in the protein of interest and that it then may be necessary to mutate a surface-accessible serine or alanine into cysteine to label the protein. This is, for instance, the case for the amyloid Hfq, where a cysteine has to be introduced (*see* **Note 3**).

3.3.2 Example of Cysteine Labeling with a Cyanine Dye

Labeling of Hfq S38C protein with Cy5-maleimide is given as an example but can be adapted to any protein or maleimide dye (*see* **Notes 2** and **3**).

1. Prepare the supplemented Washing Buffer extemporaneously with 10 mM TCEP stock solution (final TCEP concentration: 0.1 mM). TCEP is used as it interferes less with the thiol-reactive dye than DTT or β-mercaptoethanol.

2. Dissolve 1 mg of Cy5-maleimide in 30 μL DMSO. Add a twofold molar excess of Cy5-maleimide to the protein (protein concentration is usually around 1 mg/mL).
3. Incubate overnight on a rotatory shaker at 4 °C.
4. Load Ni-NTA resin with the protein (we prefer using a batch resin rather than a pre-packed column to adapt the ratio resin/protein).
5. Wash with 30 mL of washing buffer (until the solution flowing through the column becomes clear).
6. Elute with elution buffer (volume may vary depending on the volume of resin used).
7. Evaluate the protein labeling by gel electrophoresis. The gel must be imaged with a fluorescence imager (*see* **Note 4**).

3.4 Nanofluidic Stretching of DNA/Protein Complexes

1. Prior to each experiment, DNA is stained with intercalating dye YOYO-1 at a ratio of one dye molecule per ten base pairs. No anti-photo bleaching agent is used.
2. Solutions of DNA and protein are mixed and incubated overnight at 4 °C.
3. The solution of the stained DNA molecules, possibly incubated with protein, is pipetted into the loading reservoirs connected to the array of nanochannels through the microchannels. The DNA molecules, as well as protein molecules, are subsequently driven into the channels by electrophoresis. For this purpose, platinum electrodes are immersed in the reservoirs and connected to a power supply with a voltage in the range of 0.1–100 V. Once the DNA molecules are brought inside the nanochannels, the electric field is switched off, and the molecules are allowed to relax to their equilibrium state for 2–5 min.
4. Microfluidic pumps can also be used to bring the molecules inside the nanochannels.
5. Protein and DNA are visualized with an inverted fluorescence microscope with laser excitation and by using suitable dyes. Video clips with a duration of 2–5 min are recorded with an EMCCD camera. The image pixel size is calibrated with the help of a metric ruler.
6. Images are analyzed with home-developed scripts in MATLAB.

3.5 Analysis of Folding and Compaction of DNA

Amyloid proteins may play pivotal roles in the organization of the genome.

3.5.1 Experimental Setup

1. For our analysis, T4-DNA with a concentration of 3 mg of DNA/L was preincubated with the relevant protein for at least 24 h before staining with YOYO-1 dye.

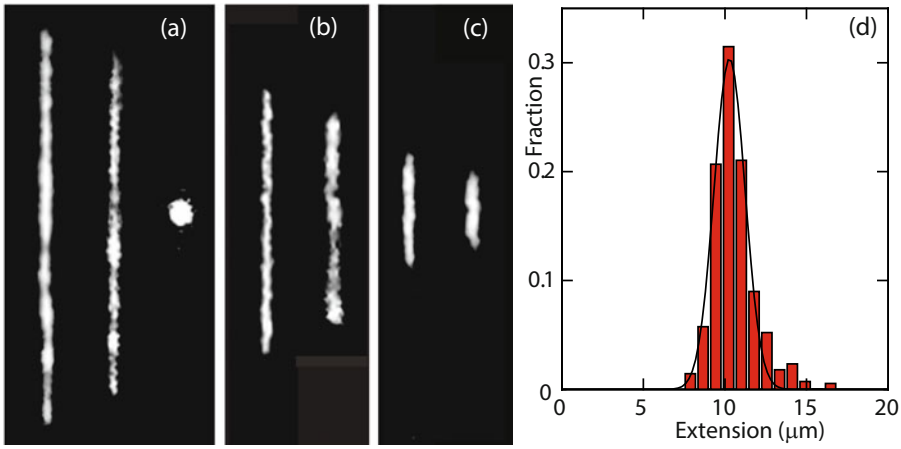

Fig. 2 (**a**) Montage of fluorescence images of T4-DNA molecules inside 150 × 250 nm^2 channels and in T-buffer. From left to right, 2×10^{-4}, 2×10^{-3}, and 3.3×10^{-1} (condensed) μM Hfq. (**b**) T4-DNA inside 200 × 300 nm^2 channels and in T-buffer with 2×10^{-4} (right) and 2×10^{-3} μM Hfq. (**c**) T4-DNA molecules inside 200 × 300 nm^2 channels and in T-buffer with 30 mM NaCl. The Hfq concentrations are 2×10^{-4} (right) and 2×10^{-3} μM. (**d**) Distribution in extension of a population of 30 molecules inside 200 × 300 nm^2 channels and in T-buffer with 2×10^{-3} μm Hfq

2. The resulting DNA-protein complexes were stretched on the array of nanochannels with electrophoresis and allowed to equilibrate for several minutes. Typical fluorescence images of the DNA molecules confined to two different channel systems and for various concentrations of Hfq are shown in Fig. 2 [9, 10].
3. We determined the average stretch along the channel for each experimental condition from an ensemble of at least 30 individual molecules (see Fig. 2d for a typical distribution in stretch). The relative stretch, that is the stretch normalized to the contour length of the DNA molecules, is set out in Fig. 3 for different examples of proteins, amyloid, or not (*see* **Note 5**).

3.5.2 Interpretation of the Conformational Response

The conformational response, as monitored by the measured stretch, depends on the protein, protein concentration, ionic strength of the supporting buffer medium, and degree of confinement (channel cross-section). For H-NS at lower ionic strength, the stretch is seen to increase with increasing protein concentration. This behavior can be attributed to DNA/H-NS filamentation, which results in an increased bending rigidity (persistence length) of the nucleoprotein fiber (a stiffer fiber is stretched to a larger extent) [11, 16]. In the case of H-NS at higher ionic strength, as well as for HU and Hfq irrespective of the ionic strength, the stretch gradually decreases with increasing protein concentration. This decrease in stretch and, hence, gradual compaction can be rationalized in a protein-mediated attractive interaction between distal DNA segments (bridging).

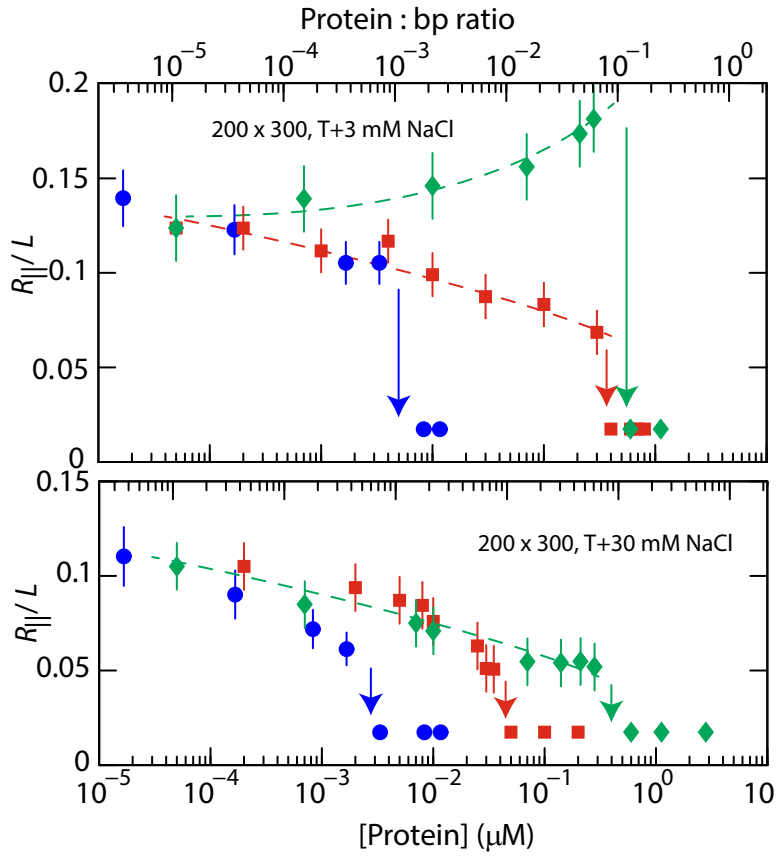

Fig. 3 Relative extension of T4-DNA inside 200 × 300 nm^2 channels versus Hfq (blue circles), HU (red squares), and H-NS (green diamonds) protein concentration. The T-buffer contains three (top panel) and 30 (bottom panel) mM NaCl. The arrows indicate the transition to a condensed form

For over-threshold concentrations of the protein, the DNA molecules collapse into a condensed form as evidenced by a bright fluorescence spot (see Fig. 2a). The critical concentration for condensation depends on the protein, buffer composition and ionic strength, and degree of confinement. With increasing channel diameter and buffer ionic strength, the thresholds shift to lower protein concentrations. This shift in condensation threshold is related to screening of excluded volume and electrostatic interaction as well as protein-mediated bridging interaction between distal DNA segments. Furthermore, these results show that the most potent condensation agent is Hfq, with threshold concentrations comparable to the ones pertaining to protamine and the polyamine spermine. This is plausibly related to bridging interaction mediated by the six protruding CTR arms. HU and H-NS are less potent with one to two orders of magnitude higher threshold concentrations. The relatively high threshold concentration for H-NS is plausibly related to the antagonistic effects of stiffening of the duplex through filamentation and protein-mediated bridging of distal DNA segments.

3.6 Measurement of Protein Target Search on DNA

Protein transport on DNA and target search are fundamental aspects of DNA metabolism (replication, repair, gene expression regulation, etc.). Accordingly, it has been widely investigated with a range of experimental methodologies and theoretical approaches. Fluorescence microscopy has allowed tracking a myriad of proteins on DNA. A single DNA substrate, on which the protein is moving, is usually aligned by flow and/or fixed in position by molecular tweezers or attached to a substrate [17–24]. Target search is facilitated by a combination of one-dimensional sliding along DNA and three-dimensional hopping and jumping between different binding sites [25–27]. An almost ignored yet important aspect of the dance of protein with DNA is the role of DNA motion and, in particular, how this is related to confinement and crowding as being critical aspects of the native, congested state [28–30].

A relatively new application of the nanofluidic device is the measurement of DNA internal motion through analysis of fluorescence correlation in conjunction with imaging and tracking of the movement of protein on DNA [12, 13]. This approach gives unprecedented information about the dynamic coupling of protein mobility and DNA motion. The methodology is based on stretching single DNA molecules on an array of long and rectangular nanofluidic channels. The channels are quasi one-dimensional and have a cross-sectional diameter of tens to a few hundreds of nanometers. This methodology can be applied to a bacterial amyloid such as Hfq.

3.6.1 Control and Measurement of DNA Segmental Motion

The first major aspect of the methodology is the control and measurement of fluctuation in DNA segment density through analysis of fluorescence correlation [12]. The workflow is illustrated in Fig. 4. First, bacteriophage λ-DNA and its dimeric and trimeric concatemers are stained with YOYO-1 dye and confined to long

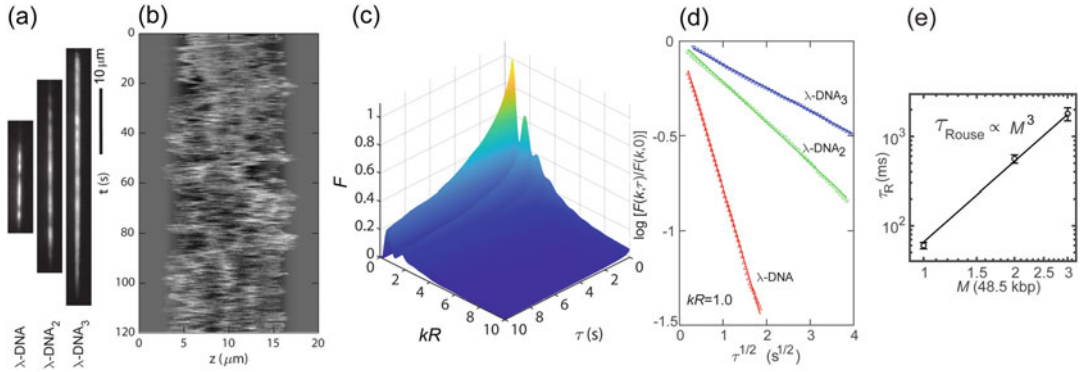

Fig. 4 (**a**) Fluorescence images of λ-DNA, dimeric λ-DNA$_2$ concatemer, and trimeric λ-DNA$_3$ concatemer confined to a 125-nm channel. (**b**) Kymograph of segmental density fluctuation for λ-DNA along the longitudinal direction of the channel. (**c**) Intermediate dynamic structure factor. (**d**) Stretched exponential fits (solid lines) to the intermediate dynamic structure factors giving DNA's relaxation time τ_R. (**e**) Rouse relaxation time τ_R vs molecular weight M in units of 48.5 kbp

and narrow nanochannels (square cross-section with a diameter of 125 nm). Images are shown in Fig. 4a. Next, video clips are recorded and analyzed to obtain the temporal fluctuation in density of the DNA segments in the longitudinal direction of the channel (Fig. 4b).

The intermediate dynamic structure factor is then derived through analysis of segment density correlation (Fig. 4c). Finally, the Rouse relaxation time pertaining to DNA internal motion is obtained from fitting the stretched exponential decay of the intermediate dynamic structure factor (Fig. 4d). Significant slowing down of DNA internal motion with relaxation times from tens of milliseconds to a few seconds with increasing DNA molecular weight was observed. The increase in relaxation time by two orders of magnitude is related to the fact that in a quasi-one-dimensional configuration, the relaxation time has a cubic dependence on the stretch (for channels of constant diameter, the stretch is proportional to molecular weight, see Fig. 4e). Accordingly, the nanofluidic device provides a unique experimental means to control and measure the DNA substrate's internal motion by manipulating its stretch.

3.6.2 Measurement of Protein Transport on DNA

The second major aspect of the methodology is to track single, fluorescence-labeled proteins, which are diffusing on a single hosting DNA molecule in the same nanochannel as applied above to quantify DNA internal motion. As an example of a DNA binding protein, we have used Hfq [13]. The method and key results are illustrated Fig. 5. Trajectories of single Hfq proteins diffusing on the various DNA concatemers were recorded and superposed on the kymograph of the DNA segmental density fluctuation (Fig. 5a). From an ensemble average of the trajectories, the corresponding protein mean square displacements were derived and are shown in Fig. 5b.

3.6.3 Interpretation of the Concerted Motion of Protein and DNA

The protein mobility shows a strong dependence on the molecular weight of the hosting DNA concatemer and, hence, DNA internal motion (see above). However, a striking and counterintuitive observation is that slower DNA motion results in much faster protein diffusion. More precisely, the diffusion coefficient of the protein was found to depend linearly on the relaxation time pertaining to DNA internal motion (Fig. 5c). This behavior was interpreted with a new diffusion model, which is based on three-dimensional diffusion through the interior of the DNA coil interspersed by periods in which the protein is immobilized in a bound state (transient, nonspecific DNA binding) [13]. These experiments showed that the residence time of Hfq bound on DNA is a key factor in determining Hfq's mobility besides DNA segments moving out of the way [30].

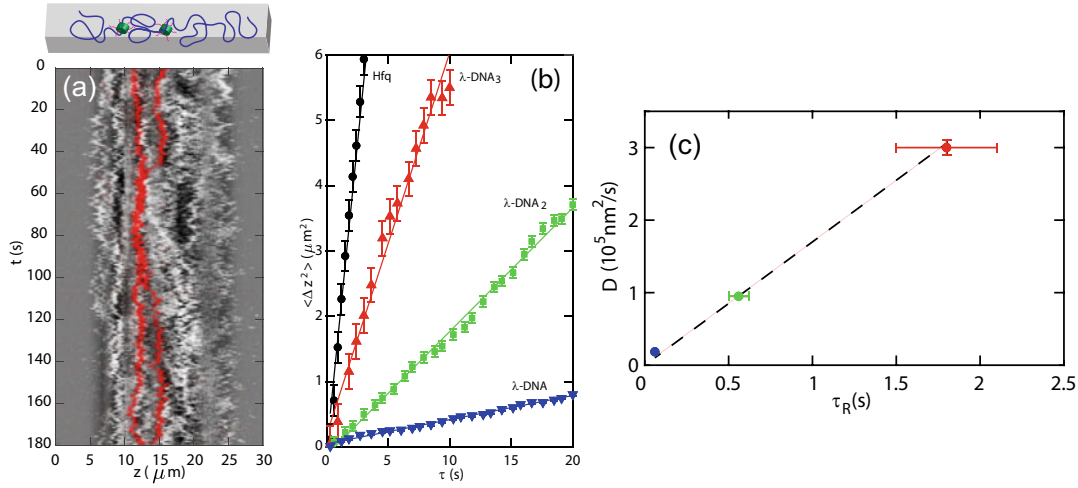

Fig. 5 (**a**) Kymograph of λ-DNA$_2$ density fluctuation (gray scale). The simultaneously recorded trajectories of two Hfq proteins diffusing on the dimeric DNA molecule are superposed in red. (**b**) Mean square displacement for Hfq (black), Hfq on λ-DNA (blue), λ-DNA$_2$ (green), and λ-DNA$_3$ (red). The solid lines represent linear fits giving the protein diffusion coefficient D. The mean square displacements were obtained with a lag-time increment (exposure time) of 300 ms. (**c**) Protein diffusion coefficient D versus DNA Rouse time τ_R for Hfq hosted by λ-DNA (blue), λ-DNA$_2$ (green), and λ-DNA$_3$ (red). The dashed line represents D proportional to τ_R variation

Thus, nanofluidics in conjunction with fluorescence microscopy presents a unique methodology to probe DNA-amyloid complexes. Miniaturization of the nanofluidic devices (smaller channel diameters) and improvements in optical imaging (sensitivity) are expected to expand further this methodology's utility for understanding the intricacies of DNA-protein interaction.

4 Notes

1. Any fluorescence-labeled maleimide bright enough for single-molecule imaging can be used. For labeling of Hfq, we obtained the best results with Cy3 cyanine dye. However, this must be optimized for each protein (*see* **Note 3**).
2. Central to the methodology is the polymer-based nanofluidic device. We present the protocol for preparing these devices and mention suppliers of the various lithographic materials as their properties are often unique. Note that the fabrication of the master stamps requires a laboratory dedicated to nanolithography.
3. The labeling position may vary, but the activity of the protein must always be checked before use. Both the introduction of the cysteine and labeling with a fluorescence dye may drastically affect the function or self-assembly of the protein. This must be optimized for each protein.

4. To evaluate the labelling efficiency, OD of the sample is measured (the blank is done on the Elution buffer). The OD is measured at 650 nm and 277 nm. OD at 277 nm corresponding to the protein is corrected from Cy5 absorption as follows: 5% of A_{650nm} is subtracted from A_{277nm} ($A_{277}{}^{corr} = A277 - 5\%A650$). [Cy5] concentration is determined using the extinction coefficient of Cy5 $\varepsilon_{650nm} = 250{,}000\ M^{-1}\ cm^{-1}$ (ε of different Cy dyes are given on GE healthcare website). [Hfq] concentration is determined using the extinction coefficient of Hfq $\varepsilon_{277nm} = 23{,}333\ M^{-1}\ cm^{-1}$. The ratio of [Cy5]/[Hfq] allows determining the labelling efficiency, which is usually >50%.
5. The examples of non-amyloid proteins such as HU and H-NS are also shown here to illustrate the difference in behaviors for other amyloids of interest that can be observed by this method (Fig. 3) [8, 11].

Acknowledgments

This work was supported by Ministry of Education, Singapore (MOE) Academic Research Fund Grants (Tier 1 R-144-000-451-114 and Tier 2 MOE-T2EP50121-00030.

References

1. Abgrall P, Nguyen NT (2008) Nanofluidic devices and their applications. Anal Chem 80: 2326–2341
2. Reisner W, Pedersen JN, Austin RH (2012) DNA confinement in nanochannels: physics and biological applications. Rep Prog Phys 75:106601. https://doi.org/10.1088/0034-4885/75/10/106601
3. van der Maarel JRC, Zhang C, van Kan JA (2014) A nanochannel platform for single DNA studies: from crowding, protein DNA interaction, to sequencing of genomic information. Isr J Chem 54:1573–1588. https://doi.org/10.1002/ijch.201400091
4. Frykholm K, Nyberg LK, Westerlund F (2017) Exploring DNA–protein interactions on the single DNA molecule level using nanofluidic tools. Integr Biol 9:650–661. https://doi.org/10.1039/C7IB00085E
5. Das SK, Austin MD, Akana MC, Deshpande P, Cao H, Xiao M (2010) Single molecule linear analysis of DNA in nanochannel labeled with sequence specific fluorescent probes. Nucleic Acids Res 38:e177–e177. https://doi.org/10.1093/nar/gkq673
6. Lam E, Hastie A, Lin C, Ehrlich D, Das S, Austin M, Deshpande P, Cao H, Nagarajan N, Xiao M, Kwok P (2012) Genome mapping on nanochannel arrays for structural variation analysis and sequence assembly. Nat Biotechnol 30:771–776
7. Basak R, Liu F, Qureshi S, Gupta N, Zhang C, de Vries R, van Kan JA, Dheen ST, van der Maarel JRC (2019) Linearization and labeling of single-stranded DNA for optical sequence analysis. J Phys Chem Lett 10:316–321. https://doi.org/10.1021/acs.jpclett.8b03465
8. Guttula D, Liu F, van Kan JA, Arluison V, van der Maarel JRC (2018) Effect of HU protein on the conformation and compaction of DNA in a nanochannel. Soft Matter 14:2322–2328. https://doi.org/10.1039/C7SM02118F
9. Jiang K, Zhang C, Guttula D, Liu F, van Kan JA, Lavelle C, Kubiak K, Malabirade A, Lapp A, Arluison V, van der Maarel JRC (2015) Effects of Hfq on the conformation and compaction of DNA. Nucleic Acids Res 43:4332–4341. https://doi.org/10.1093/nar/gkv268
10. Malabirade A, Jiang K, Kubiak K, Diaz-Mendoza A, Liu F, van Kan JA, Berret J-F, Arluison V, van der Maarel JRC (2017) Compaction and condensation of DNA mediated by the C-terminal domain of Hfq. Nucleic Acids

Res 45:7299–7308. https://doi.org/10.1093/nar/gkx431

11. Zhang C, Guttula D, Liu F, Malar PP, Ng SY, Dai L, Doyle PS, van Kan JA, van der Maarel JRC (2013) Effect of H-NS on the elongation and compaction of single DNA molecules in a nanospace. Soft Matter 9:9593. https://doi.org/10.1039/c3sm51214b
12. Yadav I, Rosencrans W, Basak R, van Kan JA, van der Maarel JRC (2020) Intramolecular dynamics of dsDNA confined to a quasi-one-dimensional nanochannel. Phys Rev Research 2:013294. https://doi.org/10.1103/PhysRevResearch.2.013294
13. Yadav I, Basak R, Yan P, van Kan JA, Arluison V, van der Maarel JRC (2020) Role of internal DNA motion on the mobility of a nucleoid-associated protein. J Phys Chem Lett 11:8424–8429. https://doi.org/10.1021/acs.jpclett.0c02251
14. van Kan JA, Bettiol AA, Watt F (2006) Proton beam writing of three-dimensional nanostructures in hydrogen silsesquioxane. Nano Lett 6: 579–582
15. van Kan JA, Zhang C, Perumal Malar P, van der Maarel JRC (2012) High throughput fabrication of disposable nanofluidic lab-on-chip devices for single molecule studies. Biomicrofluidics 6:036502. https://doi.org/10.1063/1.4740231
16. van der Maarel JRC, Guttula D, Arluison V, Egelhaaf SU, Grillo I, Forsyth VT (2016) Structure of the H-NS–DNA nucleoprotein complex. Soft Matter 12:3636–3642. https://doi.org/10.1039/C5SM03076E
17. Wang YM, Austin RH, Cox EC (2006) Single molecule measurements of repressor protein 1D diffusion on DNA. Phys Rev Lett 97: 048302. https://doi.org/10.1103/PhysRevLett.97.048302
18. Kabata H, Kurosawa O, Arai I, Washizu M, Margarson S, Glass R, Shimamoto N (1993) Visualization of single molecules of RNA polymerase sliding along DNA. Science 262: 1561–1563. https://doi.org/10.1126/science.8248804
19. Blainey PC, van Oijen AM, Banerjee A, Verdine GL, Xie XS (2006) A base-excision DNA-repair protein finds intrahelical lesion bases by fast sliding in contact with DNA. Proc Natl Acad Sci 103:5752–5757. https://doi.org/10.1073/pnas.0509723103
20. Graneli A, Yeykal CC, Robertson RB, Greene EC (2006) Long-distance lateral diffusion of human Rad51 on double-stranded DNA. Proc Natl Acad Sci 103:1221–1226. https://doi.org/10.1073/pnas.0508366103
21. Kim JH, Larson RG (2007) Single-molecule analysis of 1D diffusion and transcription elongation of T7 RNA polymerase along individual stretched DNA molecules. Nucleic Acids Res 35:3848–3858. https://doi.org/10.1093/nar/gkm332
22. Bonnet I, Biebricher A, Porté P-L, Loverdo C, Bénichou O, Voituriez R, Escudé C, Wende W, Pingoud A, Desbiolles P (2008) Sliding and jumping of single EcoRV restriction enzymes on non-cognate DNA. Nucleic Acids Res 36: 4118–4127. https://doi.org/10.1093/nar/gkn376
23. Davidson IF, Goetz D, Zaczek MP, Molodtsov MI, Huis in 't Veld PJ, Weissmann F, Litos G, Cisneros DA, Ocampo-Hafalla M, Ladurner R, Uhlmann F, Vaziri A, Peters J (2016) Rapid movement and transcriptional re-localization of human cohesin on DNA. EMBO J 35(2671–2685):10.15252/embj.201695402
24. Vestergaard CL, Blainey PC, Flyvbjerg H (2018) Single-particle trajectories reveal two-state diffusion-kinetics of hOGG1 proteins on DNA. Nucleic Acids Res 46: 2446–2458. https://doi.org/10.1093/nar/gky004
25. Hu T, Shklovskii BI (2007) How a protein searches for its specific site on DNA: the role of intersegment transfer. Phys Rev E 76: 051909. https://doi.org/10.1103/PhysRevE.76.051909
26. Gorman J, Greene EC (2008) Visualizing one-dimensional diffusion of proteins along DNA. Nat Struct Mol Biol 15:768–774. https://doi.org/10.1038/nsmb.1441
27. Mahmutovic A, Berg OG, Elf J (2015) What matters for lac repressor search in vivo—sliding, hopping, intersegment transfer, crowding on DNA or recognition? Nucleic Acids Res 43: 3454–3464. https://doi.org/10.1093/nar/gkv207
28. Mondal A, Bhattacherjee A (2015) Searching target sites on DNA by proteins: role of DNA dynamics under confinement. Nucleic Acids Res 43:9176–9186. https://doi.org/10.1093/nar/gkv931
29. Tan C, Terakawa T, Takada S (2016) Dynamic coupling among protein binding, sliding, and DNA bending revealed by molecular dynamics. J Am Chem Soc 138:8512–8522. https://doi.org/10.1021/jacs.6b03729
30. Chow E, Skolnick J (2017) DNA internal motion likely accelerates protein target search in a packed nucleoid. Biophys J 112: 2261–2270. https://doi.org/10.1016/j.bpj.2017.04.049